

A Noise-Aware Qubit Mapping Algorithm Evaluated via Qubit Interaction-Graph Criteria

Matthew Steinberg^{1,2,3}, Sebastian Feld², Carmen G. Almudever^{1,4}, Michael Marthaler³, and Jan-Michael Reiner³

¹*QuTech, Delft University of Technology, Delft, the Netherlands*

²*Quantum and Computer Engineering Department, Delft University of Technology, Delft, the Netherlands*

³*HQS Quantum Simulations GmbH, Haid-und-Neu-Straße 7, D-76131 Karlsruhe, Germany* and

⁴*Computer Engineering Department, Technical University of Valencia, Valencia, Spain*

(Dated: March 1, 2025)

The *qubit-mapping problem* aims to identify and assign qubits from a quantum circuit to a realistic NISQ device in an effort to maximize limited resources. Many algorithmic solutions for the qubit-mapping problem have been introduced, but much work remains in order to evaluate the effectiveness of a qubit-mapping algorithm with respect to mapping a quantum circuit to a device while taking into account the noise characteristics of the device. In this work, we make progress on this question in several regards. Firstly, we introduce a noise-aware heuristic mapping algorithm which fares well when compared to brute-force and trivial mapping solutions for several benchmarks. This comparison serves to provide effective upper and lower bounds for our heuristic mapper in terms of an algorithm's success rate (the estimated probability of an algorithm for successful execution on a device). Subsequently, we analyze how the performance of the mapping algorithm is affected by the characteristics of the *interaction graph*, which represents the interactions of qubits in a quantum circuit. We observe that as interaction-graph edges are added to benchmarks in either *depth-first* or *breadth-first* fashion, our heuristic algorithm's calculated success rate varies significantly, implying that both the *sheer amount* of interaction-graph vertex degree and the *distribution* of edges in a quantum circuit's interaction graph play a significant role in the calculated success rate when our greedy heuristic maps to a quantum device's coupling graph. Lastly, we discovered that our heuristic algorithm provides substantial benefits over the trivial solution when mapping quantum circuits (whose linear interaction graphs contain more than 10 qubits) to QPUs with $n \times n$ qubits under increasing n , provided that less than approximately 75% of the QPU is occupied; furthermore, as the size of the quantum processor in our simulation grows, so do the purported benefits from utilizing our heuristic mapper. This work takes the first steps towards the characterization of quantum algorithms with respect to efficient qubit-mapping solutions in NISQ-era devices.

I. INTRODUCTION

Quantum computation may still be in its infancy, but new advances have allowed for the first experimental demonstrations of quantum computing in recent years [1–5]. Quantum computers themselves promise to aid in solving classically-intractable problems for such fields as quantum chemistry [6–9], quantum machine learning [10, 11], and quantum cryptography [12, 13], among others. However, such promise comes with a catch: protecting the quantum states in a quantum computer from deleterious noise channels has proven to be a most difficult task, preventing scalability and implementations of most quantum algorithms [14]. Indeed, current prototypes of *quantum processing units* (or QPUs) available from Rigetti, Honeywell, IBM, Google, and others are considered still too resource-constrained to be able to demonstrate full fault tolerance [15–17].

In *Noisy Intermediate-Scale Quantum* (or NISQ) technology, quantum computers are still rapidly evolving and severely limited: Firstly, quantum computing as a field has not yet settled on a particular technology approach [18]; some of the leading candidate prototypes are constructed from superconducting qubits [19–24], trapped-ion qubits [25–28], as well as other contending proposals [29–33]. Secondly, most of these devices exhibit finite- and fixed-connectivity constraints between neighboring qubits (a notable exception to this is trapped-ion technology, in which one can *in principle* have "all-to-all" connectivity [25]). Thirdly, noise considerations have severely hampered developments in quantum de-

vices [34]. As such, efficient methods for executing quantum algorithms on first-generation quantum hardware require special attention.

In light of these difficulties, the goal of efficient delegation of the finite resources in a QPU for usage with near-term quantum algorithms has become exigent and pervasive. Many different approaches exist for optimizing such systems, which range widely from full-stack compilation [18] and neural-network based approaches [35, 36], to more theoretically-motivated methods such as quantum gate-synthesis techniques adapted for quantum hardware [37–40].

The present work focuses on a problem that has come to be known as the *qubit-mapping problem*. The general problem can be stated as follows: Given the finite connectivity of a NISQ-era device and its accompanying noise statistics, what is the optimal way to assign the qubits from a virtual quantum algorithm to the physical qubits of a NISQ-era processor, with some type of maximized guarantees on fidelity and/or circuit runtime? Distinct methods of solving this problem have been addressed [35, 36, 41–46]; in spite of this progress, little work has been done in order to better understand the capabilities and limitations of various qubit-mapping algorithms, especially in the case of noise awareness [44]. Due to the computational hardness of the mapping problem, one commonly resorts to heuristic solutions. It is known that in heuristic mapping algorithms, placement of the initial mapping is crucial for efficient execution of the quantum algorithm [42]; as such, we will consider only initial-mapping strategies in this work. For a review of the qubit-mapping problem, we refer the reader to

references [47, 48].

The purpose of this article is threefold: Firstly, we introduce a new heuristic mapping algorithm and benchmark it with several sets of quantum circuits. This heuristic mapping algorithm is *noise-aware*, i.e. our mapper explicitly takes into account the error-rate statistics for two-qubit, single-qubit, and measurement operations. We numerically analyze our heuristic algorithm and provide effective upper and lower bounds for its performance. These effective bounds are calculated by using two additional qubit-mapping algorithms in an effort to compare. The first of these algorithms utilizes a brute-force approach, which iterates successively through every possible mapping permutation and selects the best success rate (with respect to a metric defined in Section III C). A trivial mapper is used as the lower bound and assigns virtual qubits from a quantum circuit to a physical device in accordance with the numbering scheme used on the QPU. We observe that, for two benchmarks whose graph-theoretic representations (to be explained in Section II) admit the same vertex degree, the manner in which the two-qubit gates are distributed plays a significant role in the success rate measured, as well as the actual amount of vertex-to-vertex connections in the graph representation of the quantum circuit (we shall refer to these as *interaction graphs* as discussed in Section II); specifically, our results concern the differences between adding nonlinear edges to interaction graphs (which correspond to non-nearest neighbor two-qubit gate interactions) in both *depth-first* and *breadth-first* methods. Thirdly, we investigate the scaling properties of our heuristic algorithm for mapping quantum algorithms with nearest-neighbor two-qubit structures (such circuit properties are shown to give rise to linear interaction graphs); we find that our heuristic mapper performs well versus the trivial solution when mapping linear algorithms to large quantum-device architectures, as long as less than 75% of the device is occupied; this nontrivial performance gain is seen to not only be substantial, but to enlarge as the size of the processor itself grows, relative to the percentage of the QPU that is occupied.

The structure of this paper is as follows: Section II introduces the qubit-mapping problem in detail; we provide an instructional example to motivate our work. Section III provides details on the structure of each of the algorithms employed in this work, in addition to an explanation of how we calculated the success rate for our simulations. We separate our results in Section IV into several parts: We first describe the benchmarks utilized in our analysis in Section IV A; next, we discuss the results obtained from incorporating non-nearest-neighbor two-qubit gates in the benchmarks we tested (Section IV B), using and comparing a *breadth* versus *depth* analysis of two-qubit gate additions; and finally, in Section IV C we examine the outcomes of our simulations with large-linear interaction graphs, scaled onto QPU coupling-graphs with dimensions of $n \times n$ qubits, where $n > 3$. In Section V, we conclude our work, and discuss possible future directions for research.

II. BACKGROUND ON THE QUBIT-MAPPING PROBLEM

Most quantum circuits that are devised theoretically do not take into account the actual physical hardware constraints of a given quantum device. In order to accommodate NISQ-era hardware, quantum-programming frameworks such as Qiskit [49] include supports which allow developers to write algorithms without explicitly taking into account hardware limitations. As such, quantum compilers must perform several steps in order to prepare the quantum algorithm for actual execution on a device. Broadly speaking, these steps are: 1) to decompose the abstract quantum gates into *elementary gates*; 2) to map the qubits of the quantum circuit to the physical qubits of the quantum processor, and insert SWAP operations into the algorithm in order to satisfy the connectivity constraints of a given quantum device; 3) and to optimize the resultant quantum circuit, with an aim to minimize quantities such as the execution time and gate count, among other cost functions. The qubit-mapping problem consists of the second step of quantum compilation and will be the main focus of this article.

In the context of the qubit-mapping problem, we consider two objects: an *interaction graph*, which is a graph representation of the quantum circuit that we would like to execute (vertices represent qubits and single-qubit gates, edges two-qubit gates), and the *coupling graph*, which is a graph representation of the QPU's geometric connectivity. Most realistic QPU layouts are accompanied with *calibration* and *noise statistics* which are added to the graph; these data usually include two-qubit gate error rates, single-qubit error rates, execution times (gate length), relaxation energies, and decoherence characteristic times $T1$ and $T2$ [42]. The goal is to match the geometric connectivity of the interaction graph to that of the coupling graph as closely as possible, in our case, while regarding the noise characteristics of the device as well. In the present work, we do not directly utilize calibration statistics from a real quantum computer; instead, we have analyzed the statistics from several of the IBM quantum computers [3, 44, 50], and assume errors on the same order of magnitude (which are typically $\sim 10^2$ for single-qubit errors, and $\sim 10^3$ for two-qubit gate errors and measurement errors [44]). This procedure is discussed in detail in Section III. Additionally, several proposals show that qubits can be given *initial mappings*, which later may be modified in timestep fashion as the execution of the algorithm progresses. As the basis for this work considers only the initial-mapping portion of the qubit-mapping problem, we refer the reader to [43, 45, 46, 51] for work involving *time-scheduling techniques*.

As an instructive example, consider the quantum algorithm in Figure 1a. Before assigning qubits from the quantum algorithm to the physical QPU, the corresponding circuit is itself decomposed into a graph-theoretic form referred to as the *interaction graph*; such a decomposition is intended to visualize the action of mapping and fitting of an algorithm to a relevant portion of the QPU lattice such that the geometric constraints of the circuit are respected. As shown in Figure 1b, the resulting interaction graph is the *complete graph* K_4 , and cannot be exactly embedded into the QPU coupling graph shown in Figure 1d. In order to correctly map this algorithm, one may

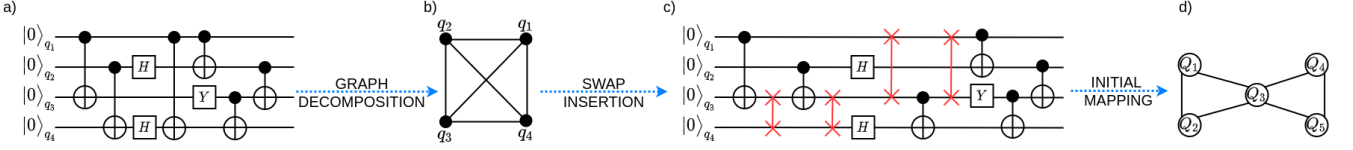


FIG. 1. a) depicts an example quantum circuit. As shown in b), this circuit is decomposed into a graph-theoretic version of the algorithm (also known as an *interaction graph*) which illustrates the interaction via two-qubit gates of qubits in the original algorithm; edges represent two-qubit gates, while vertices represent qubits which are acted upon. Weights are added to vertices and edges in order to account for more gate invocations. In c) the geometric connectivity of the interaction graph is analyzed and SWAP gates are added for any interaction-graph edges which cannot be exactly mapped to the QPU coupling graph; for example, if we define a mapping $\{q_1 \mapsto Q_1, q_2 \mapsto Q_2, q_3 \mapsto Q_3\}$, then the interaction-graph edge between q_1 and q_4 cannot be explicitly mapped, since Q_1 and Q_4 do not share an edge connection in the QPU coupling graph shown in d). The modified quantum circuit is then mapped to the QPU in d); in this way, the appropriate vertices, in accordance with some metric to be defined, are assigned to the graph-theoretic object representing the quantum device (referred to as the *coupling graph* of the QPU). In many types of qubit-mapping algorithms, qubits can then be arranged and mapped *temporally*, as well as *spatially* [42, 43, 46]; for this reason, the final arrow between c) and d) carries the designation *Initial Mapping*.

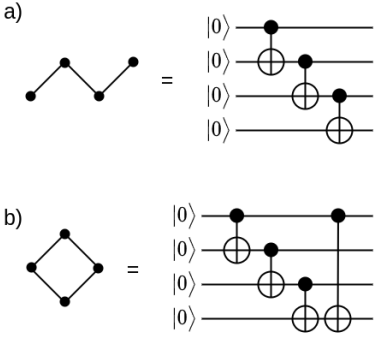


FIG. 2. In this work, we introduce the notions of interaction-graph *linearity* and *nonlinearity*. a) displays a nearest-neighbor quantum circuit, with a linear interaction graph; b) shows that adding nonlinear edges to the interaction graph is equivalent to the addition of an extra two-qubit gate, which is not nearest-neighbor in the corresponding quantum circuit.

add a SWAP gate operation to the qubits q_1 and q_3 , and then perform the required two-qubit gate between q_3 and q_4 , as depicted in the modified algorithm of Figure 1c; other SWAP gates are added as well in Figure 1. The SWAP gate itself degrades the final-state fidelity of the algorithm. Due to the disadvantageous characteristics of utilizing SWAP gates, many qubit-mapping algorithms explicitly attempt to minimize the amount of SWAP gates employed [43, 47].

The strategy described above is not the only existing approach. Indeed, solutions to the the qubit-mapping problem can be separated into two broad categories: 1) *optimal* (or brute-force) optimization and 2) heuristic optimization algorithms [47]. Additionally, most current studies of qubit-mapping focus on minimizing the number of SWAP gates [43, 47, 48, 51, 52]. However, our approach to the qubit-mapping problem is distinct because we specifically take into account NISQ-era error rates, building on the work pioneered by [44]. In literature concerning the qubit-mapping problem, this scheme is known more broadly as *noise-aware qubit mapping* [47, 48]. We will discuss the cost function utilized in this paper in Section III.

Our work additionally introduces the concepts of interaction-graph *linearity* and *nonlinearity* in the context of the qubit-mapping problem. Two examples of this idea can be seen in Figure 2. In Figure 2a, we take a four-vertex interaction graph with three edges (known as a *Hamiltonian path* P_4) to be equivalent to a four-qubit quantum circuit exhibiting nearest-neighbor two-qubit gates. As is shown in Figure 2b, if an extra edge is added, the interaction graph becomes a *cycle graph* C_4 , and corresponds to the addition of an extra two-qubit gate between the first and last qubits in the quantum circuit. In graph theory, the two objects in Figure 2 are well known; the problem of identifying suitable *Hamiltonian-path* and *cycle-graph* solutions in a simple undirected graph is related to the famous *traveling salesman problem* and is known to be NP-Complete [53–55].

In this article, we shall focus primarily on the two differing cases described above: quantum algorithms whose interaction graphs admit 1) linear and 2) nonlinear forms (disjointed interaction graphs are briefly discussed in Section IV A). The emphasis on linear interaction graphs is justified for two main reasons. Firstly, in fields such as quantum chemistry, the simulation of fermionic quantum systems can be carried out by encoding the qubits via a *Jordan-Wigner transformation* [6–8]; such an encoding scheme can give rise to circuits known as *linear SWAP networks* [56, 57], which exhibit linearity in their corresponding interaction graphs. Secondly, a quantum algorithm with a linear interacting-graph representation is, in a sense, hardware agnostic; such algorithms exhibit only nearest-neighbor two-qubit gate invocations, and are thus adaptable to any architecture. Designing a qubit-mapping algorithm for the goal of executing such algorithms was therefore paramount in our considerations. Conversely, our motivation for investigating *graph nonlinearity* as it applies to the qubit-mapping problem is not motivated necessarily with respect to realistic implementations *per se*, but rather as a method with which to understand the advantages and limitations concomitant with the design of our heuristic mapping algorithm. In this way, we qualify and quantify our greedy heuristic with respect to possible realistic implementations, in addition to addressing some advantages and limitations of our mapper. In the following section, we will detail our approach

for the qubit-mapping algorithm, specifically made with the previously-mentioned goals in mind.

III. DESCRIPTION OF THE MAPPING ALGORITHMS

All of the qubit-mapping algorithms utilized in this work generally function in the following manner: firstly, an $n \times n$ square lattice (representing the geometric connectivity of the QPU) is initialized, along with single-qubit and two-qubit error rates, as well as measurements, as a NetworkX object [58] which will serve as an approximation for the QPU device's coupling graph. Next, a quantum algorithm written in cQASM [59] is parsed into a NetworkX object as well. The qubit-mapping algorithm is then called, a final-mapping solution is assigned, and the mapping is evaluated using a cost function that is described at the end of this section (we will refer to this cost function as the *metric*). The interaction graphs used in this article for QPU simulations were mapped to coupling graphs which consist of 3×3 QPU lattice grids in the simulations from Section IV B; for the large-linear heuristic simulations of Section IV C, we map to $n \times n$ grid lattice QPUs qubits, where $n > 3$.

For all of the mapping algorithms described in this section, we will refer to an interaction graph, comprised of some set of vertices V and some set of edges E as $\tilde{C}(V, E)$; additionally, we shall refer to a QPU coupling graph with vertex set V' and edge set E' as $\tilde{Q}(V', E')$. For the algorithms that we designed, several assumptions were made:

1. If $\Delta(V) \geq \Delta(V')$ (where $\Delta(V)$ represents the *maximal vertex degree* [53]), then SWAP gates will be introduced in order to implement the proper qubit-qubit interactions for $\tilde{C}(V, E)$. We mean here that if the degree of the quantum algorithm's interaction graph exceeds the degree of the QPU's coupling graph, SWAP gates are necessitated. This assumption *does not exclude* the use of SWAP operations in the case that $\Delta(V) < \Delta(V')$; indeed, SWAP gates will almost certainly be required if the geometric connectivities of the interaction and coupling graphs do not exactly match (i.e., a graph homomorphism does not exist from the interaction graph to the QPU coupling graph [53]).
2. We additionally assume that $|V| \leq |V'|$ (where $|V|$, $|V'|$ represent the total number of vertices in the interaction and coupling graphs, respectively), i.e. that the number of vertices in the interaction graph is smaller than or equal to the number of vertices in the coupling graph. If $|V| > |V'|$, then the mapping process aborts, and an error message is displayed.

A. The Heuristic Mapping Algorithm & Traffic Coefficient

Our heuristic mapping algorithm functions as follows. After the initialization steps from the preceding paragraph are completed, our greedy-heuristic algorithm assesses the

maximum-degree vertices on the interaction graph via calculation of the *traffic coefficients*, we we will describe in more detail shortly. Next, the coupling-graph edge with the lowest error rate is identified. Afterwards, the qubit with the lowest error rate out of the two nearest-neighbor qubits is identified, and the first interaction-graph qubit is assigned to this coupling-graph qubit (the "first" interaction-graph qubit is defined as the one with the largest *maximal traffic coefficient* $\mathcal{T}_{\text{traf}}$).

The maximal traffic coefficient is calculated as follows. First, for the i^{th} interaction-graph qubit, we sum the total number of single- and two-qubit gate invocations; the *frequency* of an interaction-graph qubit is subsequently labeled f_i , as shown in Equation 1. Here, we have weighted two-qubit gate invocations ($N_{d,i}$) with an extra linear multiplier of 2 in order to weigh interaction-graph qubits which exhibit a large percentage of the two-qubit gates utilized in a given quantum algorithm more heavily than single-qubit gates; in this way, we account for *both* the nontriviality of the single-qubit gate invocations ($N_{s,i}$) and the higher error rates of two-qubit gates, which are typically at least one order of magnitude worse than for single-qubit gates [44, 50]. After a bit of algebra (Equations 2 and 3), one sees that the frequency of the i^{th} interaction-graph is re-written as a *traffic coefficient* t_i ; these traffic coefficients are summed and normalized, such that $c t_i$ provides a "percentage-wise" overview of the total interactions for the i^{th} interaction-graph qubit in an algorithm. We then take the *maximal traffic coefficient* $\mathcal{T}_{\text{traf}}$ as corresponding to the first interaction-graph qubit to be mapped, as shown in Equation 4.

$$f_i = \sum_i [N_{s,i} + 2N_{d,i}], \quad (1)$$

$$1 - \frac{1}{f_i} = t_i, \quad (2)$$

$$c \cdot \sum_i t_i = 1, \quad (3)$$

$$\max_i t_i = \mathcal{T}_{\text{traf}}, \quad (4)$$

The maximal traffic coefficient $\mathcal{T}_{\text{traf}}$ represents the percentage of interactions for the "most active" qubit in the algorithm, and is used as a way to ascertain which interaction-graph qubits must be prioritized for the best-connected, lowest error-rated portions of the QPU coupling graph via our greedy heuristic that is described in Section III A.

In order to map the rest of the interaction graph, a variant of Dijkstra's algorithm [60] is utilized, which takes into account the error rates of two- and single-qubit gates (represented on the coupling graph as edges and vertices with assigned error rates) in order to find the "shortest path" (in this case the term *shortest path* refers to the particular sequence of gates which lead to the lowest error rate, which is the shortest path, since weights are placed on the edges as two-qubit error rates) to the next available qubit in the interaction graph; once the next candidate interaction-graph qubit is designated, the algorithm surveys the interaction-graph qubits that have already been mapped. Finally, our heuristic algorithm assigns

the new candidate to the QPU coupling graph, as closely as possible (such that the least amount of errors is generated) to the originally-mapped interaction-graph qubit. This process continues until the entire algorithm has been mapped to the closest-possible qubits on the interaction graph.

B. The Brute-Force and Trivial Mapping Algorithms

The *brute-force* algorithm utilized in this work functions as follows: first, the lattice QPU is initialized, and the error rates for all quantities are defined; next, the brute-force search algorithm generates a list of all possible mapping permutations for a quantum-algorithm mapping solution. Each permutation is mapped, and is evaluated using the metric described. The preceding permutation's metric value is compared to the current iteration, and the permutation with the highest success-rate metric value is kept, while the inferior one is discarded. This process continues until the best permutation is found.

The *trivial mapping* algorithm functions by sequentially assigning interaction-graph qubits to correspondingly-numbered coupling-graph qubits; a quantum algorithm with qubits $q_1 \dots q_r$, where $r \leq n^2$ (n^2 for an $n \times n$), will be mapped to a coupling graph of a QPU with qubits $Q_1 \dots Q_s$, where $s \geq r$, by assigning interaction-/coupling-graph qubit pairs as $\{q_1 \mapsto Q_1, q_2 \mapsto Q_2, \dots, q_r \mapsto Q_r\}$. The success-rate metric is then subsequently evaluated, in order to compare with the other two mapping strategies.

C. Evaluation of the Success-Rate Metric

The cost function used to quantify the performance of all mapping algorithms in this work is described below. The purpose of this metric is to approximate the fidelity of the final quantum state after the quantum circuit is mapped and executed, with all gates invoked. Other metrics exist [43–46]; however, we limit our attention here to a metric that are based on success-rate measures.

The single-qubit gate, two-qubit gate, and SWAP-gate product metrics are calculated as shown below in Equations 5–8. These product metrics, as explained above, relate specifically to the coupling graphs that we utilize in this work.

$$\sigma_s = \prod_i^{n' < n} (1 - \xi_{s,i})^{N_{s,i}}, \quad (5)$$

$$\sigma_d = \prod_i^{\delta_d} (1 - \xi_{d,i})^{N_{d,i}}, \quad (6)$$

$$\sigma^{\text{SW}} = \prod_j^{\delta^{\text{SW}}} \prod_i^l (1 - \xi_i^{\text{SW}})^{(2Nn_i^{\text{SW}})}, \quad (7)$$

$$\sigma_{\text{total}} = \sigma_s \cdot \sigma_d \cdot \sigma^{\text{SW}}, \quad (8)$$

where on the first line, $\sigma_s, n', n, \xi_{s,i}, N_{s,i}$ are: the total single-qubit gate metric value; the total number of qubits in

the interaction graph; the total number of qubits in the coupling graph; the single-qubit gate error rate for each qubit; and the number of single-qubit gate invocations per qubit, respectively. On the second line, $\sigma_d, \delta_d, \xi_{d,i}, N_{d,i}$ are: the total two-qubit gate metric value; the total number of edges on the NISQ device; the two-qubit gate error rate per edge; and the number of two-qubit gate invocations per edge, respectively. On the final line, $\sigma^{\text{SW}}, \delta^{\text{SW}}, l, \xi_i^{\text{SW}}, 2N_i^{\text{SW}}$ represent: the total SWAP-gate metric value; the total number of separate edges that need SWAP gates; the total number of edges which physically separate the SWAP-corrected pair of coupling-graph qubits; the two-qubit gate error rate per edge; and the number of two-qubit gate invocations, for which the error rates overall are squared (this takes into account the cost of moving the qubit both to and from the closest unoccupied region, using the SWAP gate), respectively. Finally, σ_{total} represents the total metric calculated from the product of all other success rates, as mentioned above. For simplicity, we do not explicitly take into account how SWAP gates may be invoked on real QPU devices [39, 40].

Since the heuristic mapping algorithm itself functions by allocating interaction-graph qubits to coupling-graph qubits based on a measure of the success-rate, one may ask how useful it is to utilize a mapping metric based on the same measures. The reason for this can be seen as follows: when considering the optimal solution for any mapping algorithm, there are a variety of different cost functions that one may utilize. However, *any mapping* that is based on an exact calculation of the fidelity of the final quantum state after running it on a physical QPU will give the best indication of performance for a mapping solution [61]. Since direct computations of the fidelity are computationally resource-intensive and scale exponentially with the size of the QPU [14, 62], we opt to utilize a function that may be regarded as related to the calculation of the fidelity (i.e. a success rate measurement, based on the error rates as presented). In this way, we attempt to employ a cost function that is as relevant as possible, without the computational demands incurred by large-scale simulations.

In the next section, we will discuss in full the results obtained from studying several realistic interaction-graph benchmarks, benchmarks whose interaction graphs exhibit high degrees of nonlinear edges, and benchmarks which increase in size and sequentially occupy more and more of a given QPU coupling-graph's qubits.

IV. RESULTS

The results are organized as follows: Section IV A details the results obtained from realistic benchmark interaction graphs, mapped to a 3×3 coupling graph. Section IV B discusses the results from mapping quantum benchmarks with interaction graphs that exhibit increasing amounts of non-nearest neighbor two-qubit gate combinations. The results from scaling the size of linear interaction graphs onto ever-increasing QPU coupling graphs are described in Section IV C. All benchmarks were tested on a Dell Latitude 7400 laptop with a 1.9 GHz x 4 Intel i7-8665U quadcore processor

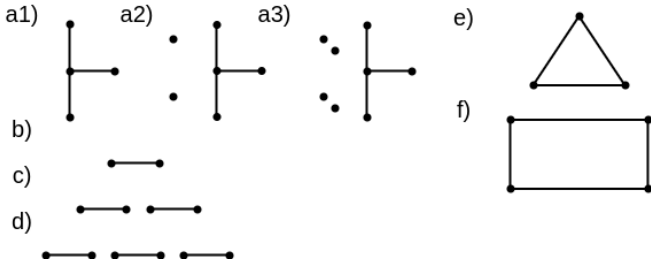


FIG. 3. Interaction graphs of several realistic benchmarks which were tested in Section IV A; the benchmarks themselves were taken from [44]. a1)-a3) show the BV4, BV6, and BV8 benchmarks, respectively; b) represents the QFT and HS2 benchmark algorithms; the interaction graphs in c) and d) were used for the HS4 and HS6 algorithms; e) depicts the Fredkin, Or, Peres, and Toffoli algorithms; and f) displays the Adder benchmark.

and 8.0 GB of RAM. Each benchmark was mapped using our simulation 100, 100, and 1000 times in Sections IV A–IV C, respectively; success rates were averaged over all trials. Simulations of Sequences I and II (as shown in Figure 5) took approximately 60 hours of continuous runtime.

A. Realistic Interaction-Graph Benchmarks

The benchmarks from [44] were utilized in this section. The corresponding interaction graphs for each of the benchmarks listed are shown in Figure 3. All of the benchmarks were tested on a 3×3 lattice coupling graph, and the results are reported in Figure 4. In this section, we did not explicitly take into account the linearity or nonlinearity of the interaction graphs; linear and nonlinear interaction-graph benchmarks will be investigated and compared in detail in Sections IV B and IV C.

The results obtained from the brute-force, heuristic-, and trivial mapping algorithms with respect to the benchmarks detailed in Figure 3 are shown in Figure 4. The algorithms themselves are grouped: the first three groupings of results pertain to the *hidden-shift algorithmic* benchmarks; the second three groupings relate the results obtained for the *Bernstein-Vazirani* benchmarks; as for the next grouping, the results belonging to the *Toffoli*, *Or*, *Fredkin*, and *Peres* benchmarks exhibit triangular interaction graphs; and finally, the *Quantum Fourier Transform* (QFT) and *Adder* benchmarks admit interaction graphs as shown in Figure 3b and Figure 3f, respectively. Red bars denote the results from the brute-force mapping algorithm; blue and green bars denote the results from the commensurate heuristic- and trivial mapping algorithms, respectively. The y-axis of Figure 4 displays the calculated success rates.

As is evidenced in the graphs, the brute-force mapping algorithm provides an effective upper bound for the performance of the heuristic mapping algorithm (we use the term *effective upper bound* with the view that better solutions may exist if one utilizes *time-scheduling techniques*, as mentioned in Section II); additionally, the trivial mapping algorithm al-

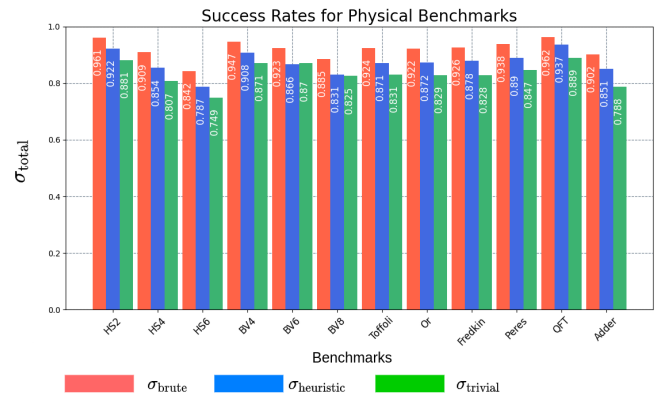


FIG. 4. Success rate for the benchmarks in [44]. Brute-force mapping results are shown in red, followed by blue and green bars, which represent the heuristic and trivial mapping results, respectively.

lows for an interpretation as an effective lower bound, with the heuristic algorithm pivoting between both of these effective bounds. Our heuristic algorithm outperforms the trivial mapping algorithm in virtually all cases except for those involving disjointness in the interaction-graph quantum algorithms, as indicated by the success-rate values of Figure 3 a2) and Figure 3 a3).

One of the main reasons for this discrepancy can be seen in the design of the heuristic mapper itself: our heuristic mapping algorithm was designed for nearest-neighbor connectivity on the interaction graph. Conversely, one can see that most of the connected interaction graphs are mapped to the coupling graph with success rates that approach the *effective upper-bounded* (brute-force) solution. Indeed, these observations indicate that a more systematic study on our heuristic mapping algorithm is warranted; in particular, one would like to have a more precise picture of how much *interaction-graph nonlinearity* our heuristic mapper can tolerate, while still providing non-trivial improvements over a trivial mapping solution.

In the following sections we will investigate these possibilities, with a focus on interaction-graph nonlinearity, as well as considering depth enlargement and the scaling of linear interaction graphs on large- n QPU coupling graphs. We will show that in particular, both the *amount* and the *distribution* of non-nearest neighbor two-qubit gates utilized in a quantum algorithm play a prominent role in determining the success rate of our heuristic mapper, relative to brute-force and trivial solutions. Moreover, we will show that our heuristic mapping algorithm outperforms the trivial-mapper for $n \times n$ QPU lattices in the regime $n > 3$.

B. Mapping Nonlinear Interaction-Graph Benchmarks

The results of this section detail a comparison between the heuristic mapping algorithm and a brute-force algorithm and trivial mapping algorithm. These two additional mapping algorithms provide *effective* upper and lower bounds on the per-

formance of the heuristic mapping algorithm, just as in the previous section. 4-, 6-, and 8-qubit interaction graphs were used as benchmarks to be mapped onto a 3×3 lattice coupling graph. Two sequences of two-qubit gate additions for 6- and 8-qubit interaction graphs are utilized, and are shown in Figure 5. We sequentially add nonlinear edges to interaction graphs, starting from their linear counterparts. Our aim is twofold: Firstly, we wish to characterize and associate the performance of our heuristic algorithm with the *amount of nonlinearity* in the corresponding interaction graph; furthermore, we secondly are interested in the *particular way* that these nonlinear edges are distributed on the interaction graph; in this section, we added nonlinear edges in *depth-first* as well as a *breadth-first* manners, and compared the two approaches. With both of these descriptors evaluated, we stand to gain a more comprehensive understanding of the advantages and limitations of our greedy heuristic as it relates to distinct interaction graphs.

In the small- n regime (for an $n \times n$ QPU coupling graph), brute-force algorithms can be utilized, as the size of the coupling and interaction graphs are sufficiently small. Even so, it must be stated that in all of our simulation results, our brute-force mapper requires several orders of magnitude longer to complete each trial than the heuristic or trivial mappers.

The sequences of nonlinear chords that were sequentially added to s -qubit linear-path interaction graphs are shown in Figure 5, where $s \in \{4, 6, 8\}$ (only one sequence of nonlinear chords is possible for 4-qubit interaction graphs, and is shown in Figure 5). Nonlinear edges are added until reaching a complete K_s graph. These edges are added as follows: in Sequence I (Figure 5), a cycle is immediately created upon adding an edge; subsequently, chords are added to the s -qubit cycle such that the degree of every sequentially-numbered vertex is maximized before proceeding to add chords to the consecutively-numbered vertices. We refer to this style of adding edges as a *depth-first* approach. Sequence II, however, exhibits a *breadth-first* approach to nonlinear-edge addition, as chords are added in a manner such that the vertex degree of all vertices remain approximately equal. The red-highlighted edges represent newly-added chords to a particular sequence. In this way, we examine and compare the effects of adding nonlinear edges (corresponding to non-nearest neighbor two-qubit gates) in two different fashions.

The results for 4-, 6-, and 8-qubit interaction graphs that were mapped in accordance with the interaction graphs in Sequence I and II are depicted in Figure 6. Figure 6a, Figure 6b and Figure 6c represent the results procured from interaction graphs in Sequence I; Figure 6d and Figure 6e represent the Sequence II results. In each subfigure, brute-force, heuristic-, and trivial mapping algorithms are shown in red, blue, and green, respectively. The success rates of each mapping algorithm $\{\sigma_{\text{brute}}, \sigma_{\text{heuristic}}, \sigma_{\text{trivial}}\}$ are graphed as a function of the number of nonlinear edges that have been added from the original sequence start in Ia4), Ia6), and Ia8) in Figure 5. The average runtime per trial for the brute-force, heuristic-, and trivial mapping algorithms are on the order of about 60 seconds for the brute-force algorithm versus 0.5 and 0.2 milliseconds for the heuristic and trivial mappers, respectively. These

figures largely stay the same for the Sequence II benchmarks, as the brute-force mapper exhibits an average solution time of several orders of magnitude higher than the other two qubit-mapping algorithms.

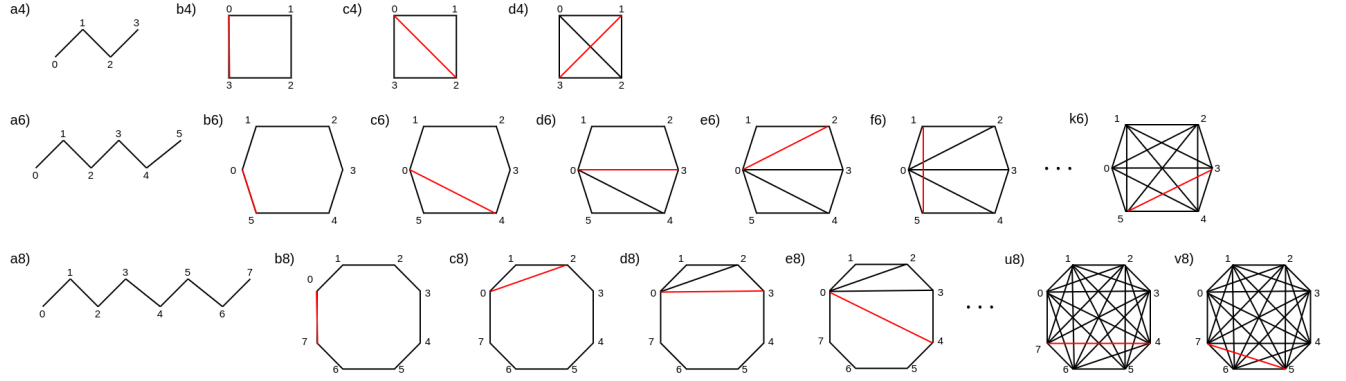
Figure 6a shows that our greedy heuristic's success rate can approach the brute-force mapper's for 4-qubit interaction graphs, no matter how much nonlinearity is added; indeed, it is observed that even a quantum algorithm representing a K_4 interaction graph can be effectively mapped to the 3×3 lattice coupling graph in our simulations. In contrast, Figure 6b and Figure 6c depict performance decreases for our heuristic optimization as more and more nonlinear edges are added to the interaction graph; Figure 6c, however, is unique in that the performance of the heuristic mapping algorithm achieves roughly analogous performance to that of the trivial mapping algorithm, until finally, after 18 nonlinear edges have been added, a "critical point" is reached. We define this critical point to be the point at which the heuristic mapping algorithm's success rate matches that of the trivial mapping algorithm's. This behavior is not witnessed in the 6-qubit interaction graphs; indeed, although the 6-qubit benchmarks do exhibit steadily-decaying performance, our results indicate that this tendency is more prevalent with larger quantum circuits, such as the 8-qubit benchmarks.

The breadth-first benchmarks of Sequence II exhibit a different trend from the first-sequence interaction graphs. Figure 6d largely appears to agree with Figure 6b; however, the second-sequence interaction graphs in Figure 6e exhibit much worse heuristic mapping success rates, compared to the first-sequence alternatives. In point of fact, the critical point occurs much more quickly while following Sequence II. Approximately 18 nonlinear edges were added in the depth-first analysis of Sequence I; in contrast, the point wherein the heuristic mapper's success rate is equal to that of the trivial mapper's is observed after approximately 7-8 nonlinear edges have been added from Sequence II (breadth-first).

Let us mention a few things here. Firstly, the data obtained from these simulations reveal that our heuristic mapper can adequately map interaction graphs which exhibit a low degree of nonlinearity, provided that the quantum circuit in question is not very deep. As we increase the sheer amount of the two-qubit gate invocations between interaction-graph qubits, it can be seen that our greedy heuristic can tolerate a small amount of interaction-graph nonlinearity, especially if this nonlinearity is concentrated only on a small subset of the total vertices. Another observation that we noted is that, for a given number of nonlinear edges added to a linear interaction graph, the success rate varies significantly for our heuristic mapper, depending on the distribution of the nonlinear edges on the interaction graphs; again, this difference suggests that not only the amount of nonlinear edges plays a role in our heuristic algorithm's calculated success rate, but also the *particular manner* in which the nonlinear edges are distributed over the interaction graph.

These same simulations were performed for the same benchmarks, with the only difference being that the number of total gates for each benchmark was multiplied by two and four. Our results largely conform with those shown in Fig-

I) SEQUENCE 1



II) SEQUENCE 2

FIG. 5. Interaction graphs for the first and second benchmark sequences. Red edges depict newly-added nonlinear edges to the interaction graphs that were tested with our greedy heuristic. In the interaction graphs from Sequence I, nonlinear edges are appended such that every vertex degree is maximized before subsequently appending nonlinear edges to consecutively higher-numbered vertices; this process continues until a K_s graph is attained for Sequence I (We refer to this technique as a *depth-first* edge-assignment procedure). As for Sequence II, a *breadth-first* edge-assignment procedure is utilized, as nonlinear edges are appended such that every vertex exhibits approximately the same degree until a K_s graph is reached.

ure 6, as only the scaling of the success-rate metric changes. This observation is indeed expected, as the design of the experiment and the cost function themselves facilitate such a rescaling.

Lastly, as shown in Figure 6c and Figure 6e, the heuristic's and trivial mapper's success rates are relatively close. One may surmise that a reason for this proximity may be in fact related to the high occupancy of the coupling-graph qubits during our simulations (8/9 of the available QPU qubits were utilized). The next section will provide information related to the large-linear interactions graphs that were tested and how they scale in the regime $n > 3$ for a corresponding $n \times n$ QPU coupling graph. We specifically address the question of how the occupancy percentage of the QPU affects our mapper's solution.

C. Scaling Properties in the Regime $n > 3$

The benchmarks tested in this section are all linear, but vary in size so as to occupy different percentages of an $n \times n$ QPU coupling graph, where $n = 3, \dots, 10$. A coupling graph of lattice dimensions $n \times n$ is initialized, and sequentially larger and larger linear interaction graphs are mapped to a coupling

graph until it is 100% occupied; as in the previous simulations, vertices of the coupling graph are taken to be qubits. Additionally, no explicit noise scaling was utilized as the coupling graph increases; the magnitudes of noise for two-qubit and single-qubit error rates, as well as measurements are kept the same as described in Section III. As brute-force algorithms were not utilized for this section (becoming practically intractable if $n > 3$), success rates were instead compared between the heuristic and trivial mappers, as shown in Figure 7b and Figure 7c.

The results from our study are displayed in Figure 7. Figure 7a shows the success-rate difference $\{\sigma_{\text{heuristic}} - \sigma_{\text{trivial}}\}$, calculated between our greedy heuristic and the trivial mapper, with respect to linear interaction graphs that progressively fill the entire QPU coupling graph. The different colors in Figure 7a denote differing n -values for the lattice dimensions of the coupling graph. Figure 7b and Figure 7c display the actual success rates calculated under no noise scaling behavior, for 4×4 and 6×6 coupling-graph dimensions, respectively.

In these graphs, one can observe several trends: firstly, as the n -value of the coupling graph increases, the success-rate difference becomes steadily larger for linear interaction graphs that occupy the same percentage of the coupling graph when fully mapped, until about 75% of the QPU is occu-

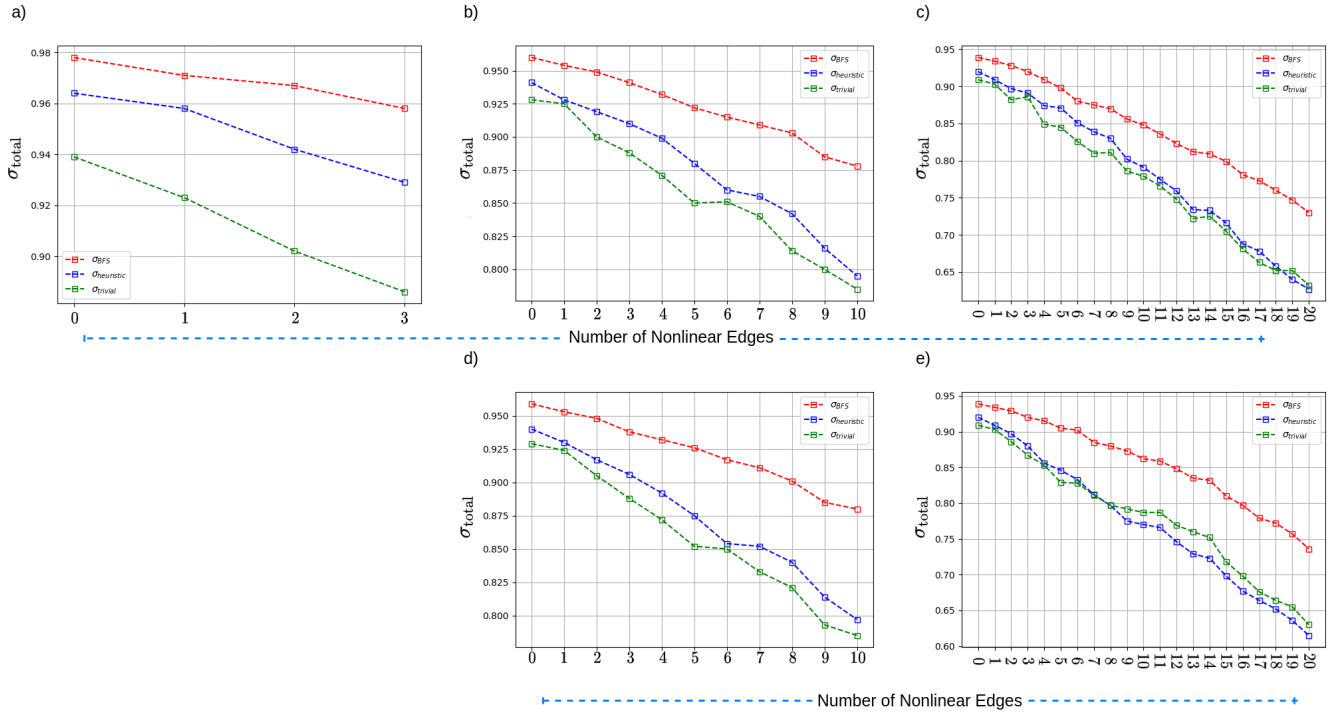


FIG. 6. a)-c) show the results for the nonlinear benchmarks in Figure 5 for Sequence I (the depth-first benchmarks); the x-axis of the figure follows the sequence of nonlinear-edge additions. The average runtime per trial for all of the benchmarks was approximately 60 seconds, 0.5, and 0.2 milliseconds for the brute-force, heuristic, and the trivial mapping algorithms, respectively. The total runtime for the entire simulation was approximately 60 hours. d)-e) show the results for the nonlinear benchmark interaction graphs in Figure 5 for Sequence II. These breadth-first benchmarks exhibited an average runtime per trial were approximately equal to those stated for the depth-first benchmarks.

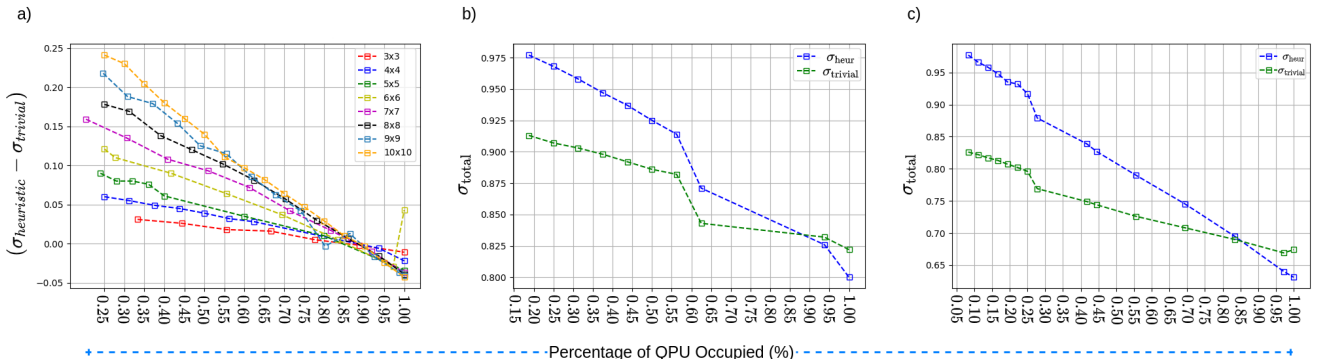


FIG. 7. Success-rate differences between the success rates of the heuristic and trivial mappings ($\sigma_{\text{heuristic}}$, σ_{trivial}) taken from n -qubit linear interaction graphs which have been mapped to $n \times n$ QPU coupling graphs. a) displays the success rates differences without any noise scaling. b) and c) detail the success rate σ_{total} calculated for both $n = 4$ and $n = 6$ QPU coupling graphs, respectively.

pied. Next, after approximately 75% of the coupling graph has been filled, the success-rate difference becomes negligible; this success-rate difference implies that an effectively negligible difference between the heuristic- and the trivial mapping algorithms is observed. Lastly, after roughly 85 – 90% of the lattice coupling graph is occupied, the success-rate difference is not only negligible, but starts to dip below zero, the main observation here being that the greedy heuristic cannot find a solution that outperforms the success rate measured from the trivial mapper. We will discuss the consequences of this ob-

servation in Section V.

Additionally, we performed the same tests for coupling graphs with increasing n -values such that a uniform increase in noise of order 4 times larger than the noise in Figure 7, as well as under exponentially increasing noise. The purpose of these rescaled-noise simulations was to investigate potentially more realistic noise, as device error rates are expected to increase due to crosstalk as quantum processors become larger [50, 63]. Our results from these simulations largely confirm the same trends that were mentioned in the preceding para-

graphs, albeit with steeper linear decays.

In the last section, we will summarize our main results. Particular emphasis will be placed on interpreting the observations noted in the previous sections. We will then close by highlighting some future research directions.

V. DISCUSSION & FUTURE WORK

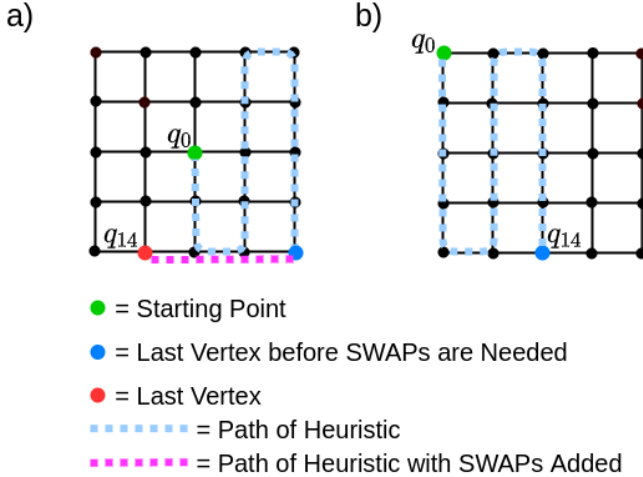


FIG. 8. An example scenario in which our heuristic mapping algorithm could perform worse in comparison to a trivial mapping algorithm. On the 5×5 coupling graph pictured above, a) and b) represent possible final-mapping solutions for the heuristic- and trivial mapping algorithms, respectively. In a), one may initiate the mapping process in a highly-connected region of the coupling graph; however, as one proceeds using the algorithm to consecutively map the 15 qubits in our quantum-circuit example, one may encounter a situation in which the heuristic-based solution may involve several more SWAP gates than normally anticipated. This situation is shown as a dotted line in blue (tracing out the nearest-neighbor assignment path of our heuristic) which essentially runs into a corner in the lower-right portion of the QPU coupling graph, stopping at the vertex shown in blue. From this point forward, the next shortest-path distance would not be a nearest-neighbor vertex, and SWAPs will undoubtedly be needed in order to realize such a mapping solution (shown by the dotted line in magenta, which terminates at the red-labelled vertex q_{14}). In b), a trivial mapping solution would better utilize the space and connectivity available for a QPU when less choices are available.

In this article, we have introduced a heuristic qubit-mapping algorithm for the purpose of exploring the advantages and limitations for mapping different types of interaction graphs. The heuristic algorithm itself is *noise-aware*, and the success rate is high, relative to a brute-force and trivial mapper, which serve to effectively bound the performance of our heuristic from above and below. For small, low-depth quantum circuits, our heuristic is shown to provide a significant performance gain over a trivial mapping solution, and in some cases for realistic benchmarks even approaches that of a brute-force mapping algorithm. As the main motivation for this work concerned investigations of *connected interaction graphs*, we did not explicitly think of ways to correct the issue with disjointed interaction-graph success rates; we reserve such explorations for future work. With this work, we have taken the first step towards characterizing interaction graphs of quantum circuits which admit amenable mapping solutions, specifically for a particular mapping algorithm.

We have accomplished this initiative in two main stages: Firstly, we have investigated the performance of our brute-force, heuristic, and trivial mappers with low-depth quantum circuits which admit nonlinear interaction graphs. Two particular sequences of non-nearest neighbor two-qubit gate additions were considered, both of which highlight the inherent limitations of the heuristic mapping algorithm that we devised. The manner in which nonlinear edges are added to the circuit (i.e. depth-first or breadth-first), as well as the sheer amount of nonlinear edges utilized, both were found to play a role in our greedy heuristic's calculated success rate. These two observations are evidenced from an analysis of Figure 6c and Figure 6e: although our heuristic mapper performs better than the trivial mapping for most of the depth-first edge additions (Sequence I), we see that the performance is *not much better*, implying that our heuristic can tolerate a relatively low amount of interaction-graph nonlinearity, in the case of the number of qubits in the interaction graph being relatively high. This observation comes as no surprise, seeing as the algorithm was designed to accommodate linear interaction graphs. Furthermore, for two interaction graphs with the same number of nonlinear edges, it was found that our heuristic mapper's performance largely depends on the particular manner in which the nonlinear interaction-graph edges are distributed. We verified that this fact is reinforced for deeper algorithms by running simulations with larger-depth interaction graphs of the same form as described in Figure 5.

Secondly, we investigated the scaling behavior of our heuristic mapping algorithm in the regime $n > 3$ for $n \times n$ QPU coupling graphs. In this regime, our brute-force solutions to the mapping problem become intractable; as such, our heuristic mapper was compared to the trivial mapper described in Section III. The results indicate that the greedy heuristic scales well for quantum circuits with linear interaction graphs, as long as less than approximately 75% of the QPU coupling graph is filled (in comparison to our trivial mapper). If one occupies more of the available space on the QPU, one can expect a trivial benefit from utilizing our heuristic mapper, until approximately 85% of the processor is allocated; after this marker, performance losses can be expected (with respect to our trivial mapper), as our results denoted. Additionally, for comparable percentages of the coupling graph that are filled, one can expect higher success rates relative to the trivial mapping solution as n is steadily increased. These same simulations were additionally employed for uniformly and exponentially increasing noise parameters, concomitant with observations that larger QPU devices experience more problems with error rates due to crosstalk [50, 63]. Our results confirm and reinforce the remarks stated above.

A few final comments are in order here. In reference to the results from Section IV C, one may ask why our heuris-

tic mapping algorithm tends to underperform as we occupy larger percentages of a QPU coupling graph. An answer to this question can be seen when one considers that, as the coupling graph is filled up, less and less nearest-neighbor choices are left for the heuristic algorithm to evaluate. As the algorithm itself functions by selecting first the minimum error-rate vertex of the minimal error-rate edge from the supremum of vertex degrees, the heuristic-based solution will necessitate more SWAP gates as the processor is further allocated. In this regime (i.e. when over 75% of the QPU is occupied), the trivial mapping algorithm used in this study would be expected to outperform the our heuristic mapper for quantum circuits that give rise to linear interaction graphs.

An example of just such a difficulty is explained in more detail in Figure 8; indeed, in a) and b), one sees the result of a greedy shortest-path mapper applied to a 5×5 coupling graph. In Figure 8a, we may start with a high-degree vertex (shown in green); as the algorithm proceeds to find nearest-neighbor solutions, the algorithm's attempt to map the 15-qubit linear interaction graph in our example may run into a portion of the device that is less-highly connected (shown by the blue-dotted line which terminates at the blue-labelled vertex). When such an event happens, our heuristic will continue searching for the nearest possible neighbor that is free; unfortunately, in this case several SWAP gates would be needed in order to realize the mapping shown (denoted by the magenta-dotted line that terminates at the red vertex q_{14}). In Figure 8b, we see an example of our trivial mapping algorithm would make better use of the space requirements for the 15-qubit quantum circuit. One solution to this issue with our heuristic may be to utilize *look-ahead* or *look-behind* techniques, which would serve to match not only the nearest neighbor on the coupling graph, but to additionally analyze several interaction-graph vertices [52, 64, 65]. Such a qubit-mapping algorithm may improve overall success rates; in any case, we leave further discussion of this possibility to future work.

As a final comment, it was observed that our brute-force mapping algorithm scaled badly after $n = 3$ for the coupling graphs tested; this does not necessarily imply that *any exact simulation* is intractable. Although we note that finding an exact solution to the qubit-mapping problem is NP-hard, one may be able to write an exact mapping algorithm which does in fact scale better than ours for larger n -values.

Admittedly, there are still many avenues left for possible investigation in the future, as much work needs to be done in order to better characterize and/or match quantum algorithms to prospective qubit mappers. One may investigate more sophisticated heuristic and exact algorithms, as there is certainly room for improvement over the heuristic mapping algorithm that we have presented here. Additionally, one may analyze more realistic noise conditions, in addition to more realistic QPU coupling graphs, as the authors in [47] propose. Various other qubit-mapping algorithm proposals exist as well [35, 36, 41–43, 45, 46]; many of these could be analyzed and classified as well. We intend to investigate these possibilities in future work.

VI. ACKNOWLEDGEMENTS

We thank Jens Eisert for fruitful discussions. MS would like to thank HQS Quantum Simulations GmbH, where a portion of this work was completed.

[1] F. Arute, K. Arya, R. Babbush, D. Bacon, J. C. Bardin, R. Barends, R. Biswas, S. Boixo, F. G. S. L. Brandao, D. A. Buell, and et al., Quantum supremacy using a programmable superconducting processor, *Nature* **574**, 505–510 (2019).

[2] D. Leibfried, R. Blatt, C. Monroe, and D. Wineland, Quantum dynamics of single trapped ions, *Rev. Mod. Phys.* **75**, 281 (2003).

[3] P. Jurcevic, A. Javadi-Abhari, L. S. Bishop, I. Lauer, D. F. Bogorin, M. Brink, L. Capelluto, O. Günlük, T. Itoko, N. Kanazawa, A. Kandala, G. A. Keefe, K. Krsulich, W. Landers, E. P. Lewandowski, D. T. McClure, G. Nannicini, A. Narasgond, H. M. Nayfeh, E. Pritchett, M. B. Rothwell, S. Srinivasan, N. Sundaresan, C. Wang, K. X. Wei, C. J. Wood, J.-B. Yau, E. J. Zhang, O. E. Dial, J. M. Chow, and J. M. Gambetta, Demonstration of quantum volume 64 on a superconducting quantum computing system (2020), arXiv:2008.08571 [quant-ph].

[4] H.-S. Zhong, H. Wang, Y.-H. Deng, M.-C. Chen, L.-C. Peng, Y.-H. Luo, J. Qin, D. Wu, X. Ding, Y. Hu, P. Hu, X.-Y. Yang, W.-J. Zhang, H. Li, Y. Li, X. Jiang, L. Gan, G. Yang, L. You, Z. Wang, L. Li, N.-L. Liu, C.-Y. Lu, and J.-W. Pan, Quantum computational advantage using photons, *Science* **370**, 1460 (2020), <https://science.sciencemag.org/content/370/6523/1460.full.pdf>.

[5] J. M. Pino, J. M. Dreiling, C. Figgatt, J. P. Gaebler, S. A. Moses, M. S. Allman, C. H. Baldwin, M. Foss-Feig, D. Hayes, K. Mayer, C. Ryan-Anderson, and B. Neyenhuis, Demonstration of the QCCD trapped-ion quantum computer architecture, arXiv e-prints , arXiv:2003.01293 (2020), arXiv:2003.01293 [quant-ph].

[6] J.-M. Reiner, F. Wilhelm-Mauch, G. Schön, and M. Marthaler, Finding the ground state of the hubbard model by variational methods on a quantum computer with gate errors, *Quantum Science and Technology* **4**, 035005 (2019).

[7] J.-M. Reiner, S. Zanker, I. Schwenk, J. Leppäkangas, F. Wilhelm-Mauch, G. Schön, and M. Marthaler, Effects of gate errors in digital quantum simulations of fermionic systems, *Quantum Science and Technology* **3**, 045008 (2018).

[8] S. McArdle, S. Endo, A. Aspuru-Guzik, S. C. Benjamin, and X. Yuan, Quantum computational chemistry, *Reviews of Modern Physics* **92**, 10.1103/revmodphys.92.015003 (2020).

[9] T. R. Bromley, J. M. Arrazola, S. Jahangiri, J. Izaac, N. Quesada, A. D. Gran, M. Schuld, J. Swinarton, Z. Zabaneh, and N. Killoran, Applications of near-term photonic quantum computers: software and algorithms, *Quantum Science and Technology* **5**, 034010 (2020).

[10] J. Biamonte, P. Wittek, N. Pancotti, and et al., Quantum machine learning, *Nature* **549**, 195–202 (2017).

[11] V. Dunjko and H. J. Briegel, Machine learning & artificial intelligence in the quantum domain: a review of recent progress, *Reports on Progress in Physics* **81**, 074001 (2018).

[12] N. Gisin, G. Ribordy, W. Tittel, and H. Zbinden, Quantum cryptography, *Rev. Mod. Phys.* **74**, 145 (2002).

[13] S. Pirandola, U. L. Andersen, L. Banchi, M. Berta, D. Bunnadar, R. Colbeck, D. Englund, T. Gehring, C. Lupo, C. Ottaviani, and et al., Advances in quantum cryptography, *Advances in Optics and Photonics* **12**, 1012 (2020).

[14] J. Preskill, Quantum Computing in the NISQ era and beyond, *Quantum* **2**, 79 (2018).

[15] S. J. Devitt, W. J. Munro, and K. Nemoto, Quantum error correction for beginners, *Reports on Progress in Physics* **76**, 076001 (2013).

[16] L. Egan, D. M. Debroy, C. Noel, A. Risinger, D. Zhu, D. Biswas, M. Newman, M. Li, K. R. Brown, M. Cetina, and C. Monroe, Fault-Tolerant Operation of a Quantum Error-Correction Code, arXiv e-prints , arXiv:2009.11482 (2020), arXiv:2009.11482 [quant-ph].

[17] N. M. Linke, M. Gutierrez, K. A. Landsman, C. Figgatt, S. Debnath, K. R. Brown, and C. Monroe, Fault-tolerant quantum error detection, *Science Advances* **3**, e1701074 (2017).

[18] P. Murali, N. M. Linke, M. Martonosi, A. J. Abhari, N. H. Nguyen, and C. H. Alderete, Full-stack, real-system quantum computer studies: Architectural comparisons and design insights, in *Proceedings of the 46th International Symposium on Computer Architecture*, ISCA '19 (Association for Computing Machinery, New York, NY, USA, 2019) p. 527–540.

[19] J. You and F. Nori, Atomic physics and quantum optics using superconducting circuits, *Nature* **474**, 589–597 (2011).

[20] C. Neill, P. Roushan, K. Kechedzhi, S. Boixo, S. V. Isakov, V. Smelyanskiy, A. Megrant, B. Chiaro, A. Dunsworth, K. Arya, R. Barends, B. Burkett, Y. Chen, Z. Chen, A. Fowler, B. Foxen, M. Giustina, R. Graff, E. Jeffrey, T. Huang, J. Kelly, P. Klimov, E. Lucero, J. Mutus, M. Neeley, C. Quintana, D. Sank, A. Vainsencher, J. Wenner, T. C. White, H. Neven, and J. M. Martinis, A blueprint for demonstrating quantum supremacy with superconducting qubits, *Science* **360**, 195 (2018), <https://science.sciencemag.org/content/360/6385/195.full.pdf>.

[21] R. Barends, J. Kelly, A. Megrant, and et al., Superconducting quantum circuits at the surface code threshold for fault tolerance, *Nature* **508**, 500–503 (2014).

[22] H. Huang, D. Wu, D. Fan, and et al., Superconducting quantum computing: a review, *Sci. China Inf. Sci.* **63**, 180501 (2020).

[23] A. Wallraff, D. Schuster, A. Blais, and et al., Strong coupling of a single photon to a superconducting qubit using circuit quantum electrodynamics, *Nature* **431**, 162–167 (2004).

[24] E. A. Sete, W. J. Zeng, and C. T. Rigetti, A functional architecture for scalable quantum computing, in *2016 IEEE International Conference on Rebooting Computing (ICRC)* (2016) pp. 1–6.

[25] C. D. Bruzewicz, J. Chiaverini, R. McConnell, and J. M. Sage, Trapped-ion quantum computing: Progress and challenges, *Applied Physics Reviews* **6**, 021314 (2019).

[26] P. Schindler, D. Nigg, T. Monz, J. T. Barreiro, E. Martinez, S. X. Wang, S. Quint, M. F. Brandl, V. Nebendahl, C. F. Roos, and et al., A quantum information processor with trapped ions, *New Journal of Physics* **15**, 123012 (2013).

[27] J. I. Cirac and P. Zoller, Quantum computations with cold trapped ions, *Phys. Rev. Lett.* **74**, 4091 (1995).

[28] T. Monz, P. Schindler, J. T. Barreiro, M. Chwalla, D. Nigg, W. A. Coish, M. Harlander, W. Hänsel, M. Hennrich, and R. Blatt, 14-qubit entanglement: Creation and coherence, *Physical Review Letters* **106**, 10.1103/physrevlett.106.130506 (2011).

[29] R. Maurand, X. Jehl, D. Kotekar-Patil, and et al., A cmos silicon spin qubit, *Nature Communications* **7**, 13575 (2016).

[30] S. Slussarenko and G. J. Pryde, Photonic quantum information processing: A concise review, *Applied Physics Reviews* **6**, 041303 (2019).

[31] J. E. Bourassa, R. N. Alexander, M. Vasmer, A. Patil, I. Tzitrin, T. Matsuura, D. Su, B. Q. Baragiola, S. Guha, G. Dauphinais, and et al., Blueprint for a scalable photonic fault-tolerant quantum

tum computer, *Quantum* **5**, 392 (2021).

[32] S. Bartolucci, P. Birchall, H. Bombin, H. Cable, C. Dawson, M. Gimeno-Segovia, E. Johnston, K. Kieling, N. Nickerson, M. Pant, F. Pastawski, T. Rudolph, and C. Sparrow, Fusion-based quantum computation (2021), arXiv:2101.09310 [quant-ph].

[33] C. Chamberland, K. Noh, P. Arrangoiz-Arriola, E. T. Campbell, C. T. Hann, J. Iverson, H. Putterman, T. C. Bohdanowicz, S. T. Flammia, A. Keller, G. Refael, J. Preskill, L. Jiang, A. H. Safavi-Naeini, O. Painter, and F. G. S. L. Brandão, Building a fault-tolerant quantum computer using concatenated cat codes (2020), arXiv:2012.04108 [quant-ph].

[34] E. Knill, Quantum computing with realistically noisy devices, *Nature* **434**, 39–44 (2005).

[35] S. Herbert and A. Sengupta, Using reinforcement learning to find efficient qubit routing policies for deployment in near-term quantum computers (2019), arXiv:1812.11619 [quant-ph].

[36] M. G. Pozzi, S. J. Herbert, A. Sengupta, and R. D. Mullins, Using reinforcement learning to perform qubit routing in quantum compilers (2020), arXiv:2007.15957 [quant-ph].

[37] V. Shende, S. Bullock, and I. Markov, Synthesis of quantum-logic circuits, *IEEE Transactions on Computer-Aided Design of Integrated Circuits and Systems* **25**, 1000–1010 (2006).

[38] M. Saeedi and I. L. Markov, Synthesis and optimization of reversible circuits—a survey, *ACM Comput. Surv.* **45**, 10.1145/2431211.2431220 (2013).

[39] M. Saeedi, R. Wille, and R. Drechsler, Synthesis of quantum circuits for linear nearest neighbor architectures, *Quantum Inf Process* **10**, 355–377 (2011).

[40] P. Niemann, R. Wille, and R. Drechsler, Efficient synthesis of quantum circuits implementing clifford group operations, in *2014 19th Asia and South Pacific Design Automation Conference (ASP-DAC)* (2014) pp. 483–488.

[41] P. Narang, W. Finigan, M. Cubeddu, and J. Flick, Qubit allocation for noisy intermediate-scale quantum computers (2020).

[42] S. Niu, A. Suau, G. Staffelbach, and A. Todri-Sanial, A hardware-aware heuristic for the qubit mapping problem in the nisq era, *IEEE Transactions on Quantum Engineering* **1**, 1 (2020).

[43] L. Lao, D. Manzano, H. van Someren, I. Ashraf, and C. G. Almudéver, Mapping of quantum circuits onto nisq superconducting processors, arXiv: Quantum Physics (2019).

[44] P. Murali, J. M. Baker, A. Javadi-Abhari, F. T. Chong, and M. Martonosi, Noise-adaptive compiler mappings for noisy intermediate-scale quantum computers, in *Proceedings of the Twenty-Fourth International Conference on Architectural Support for Programming Languages and Operating Systems, ASPLOS ’19* (Association for Computing Machinery, New York, NY, USA, 2019) p. 1015–1029.

[45] D. Venturelli, M. Do, E. Rieffel, and J. Frank, Compiling quantum circuits to realistic hardware architectures using temporal planners, *Quantum Science and Technology* **3**, 025004 (2018).

[46] A. Cowtan, S. Dilkes, R. Duncan, A. Krajenbrink, W. Simmons, and S. Sivarajah, On the Qubit Routing Problem, in *14th Conference on the Theory of Quantum Computation, Communication and Cryptography (TQC 2019)*, Leibniz International Proceedings in Informatics (LIPIcs), Vol. 135, edited by W. van Dam and L. Mancinska (Schloss Dagstuhl–Leibniz-Zentrum fuer Informatik, Dagstuhl, Germany, 2019) pp. 5:1–5:32.

[47] M. Bandic, H. Zarein, E. Alarcon, and C. G. Almudever, On structured design space exploration for mapping of quantum algorithms, in *2020 XXXV Conference on Design of Circuits and Integrated Systems (DCIS)* (2020) pp. 1–6.

[48] C. G. Almudever, L. Lao, R. Wille, and G. G. Guerreschi, Realizing quantum algorithms on real quantum computing devices, in *2020 Design, Automation Test in Europe Conference Exhibition (DATE)* (2020) pp. 864–872.

[49] H. Abraham, AduOffei, R. Agarwal, I. Y. Akhalwaya, G. Aleksandrowicz, T. Alexander, M. Amy, E. Arbel, Arijit02, A. Asfaw, A. Avkhadiev, C. Azaustre, AzizNgoueya, A. Banerjee, A. Bansal, P. Barkoutsos, A. Barnawal, S. Bravyi, Bryce-Fuller, D. Bucher, and A. B. et al., Qiskit: An open-source framework for quantum computing (2019).

[50] P. Murali, D. C. Mckay, M. Martonosi, and A. Javadi-Abhari, Software mitigation of crosstalk on noisy intermediate-scale quantum computers, *Proceedings of the Twenty-Fifth International Conference on Architectural Support for Programming Languages and Operating Systems* 10.1145/3373376.3378477 (2020).

[51] B. Tan and J. Cong, Optimality study of existing quantum computing layout synthesis tools, *IEEE Transactions on Computers* , 1–1 (2020).

[52] A. Zulehner, A. Paler, and R. Wille, An efficient methodology for mapping quantum circuits to the ibm qx architectures, *IEEE Transactions on Computer-Aided Design of Integrated Circuits and Systems* **38**, 1226 (2019).

[53] R. J. Wilson, *Introduction to Graph Theory* (John Wiley & Sons, Inc., USA, 1986).

[54] C. H. Papadimitriou and K. Steiglitz, *Combinatorial Optimization: Algorithms and Complexity* (Prentice-Hall, Inc., USA, 1982).

[55] D. Ferrari, I. Tavernelli, and M. Moretti, Deterministic Algorithms for Compiling Quantum Circuits with Recurrent Patterns, arXiv e-prints , arXiv:2102.08765 (2021), arXiv:2102.08765 [quant-ph].

[56] I. D. Kivlichan, J. McClean, N. Wiebe, C. Gidney, A. Aspuru-Guzik, G. K.-L. Chan, and R. Babbush, Quantum simulation of electronic structure with linear depth and connectivity, *Physical Review Letters* **120**, 10.1103/physrevlett.120.110501 (2018).

[57] B. O’Gorman, W. J. Huggins, E. G. Rieffel, and K. B. Whaley, Generalized swap networks for near-term quantum computing (2019), arXiv:1905.05118 [quant-ph].

[58] A. Hagberg, P. Swart, and D. Chult, Exploring network structure, dynamics, and function using networkx (2008).

[59] N. Khammassi, G. Guerreschi, I. Ashraf, J. Hogaboam, C. G. Almudéver, and K. Bertels, cqasm v1.0: Towards a common quantum assembly language, arXiv: Quantum Physics (2018).

[60] E. W. Dijkstra, A note on two problems in connexion with graphs, *Numer. Math.* **1**, 269–271 (1959).

[61] S. Nishio, Y. Pan, T. Satoh, H. Amano, and R. V. Meter, Extracting success from ibm’s 20-qubit machines using error-aware compilation, *J. Emerg. Technol. Comput. Syst.* **16**, 10.1145/3386162 (2020).

[62] M. A. Nielsen and I. L. Chuang, *Quantum Computation and Quantum Information: 10th Anniversary Edition* (Cambridge University Press, 2010).

[63] D. Hangleiter, Crosstalk diagnosis for the next generation of quantum processors, *Quantum Views* **4**, 46 (2020).

[64] R. Wille, O. Keszocze, M. Walter, P. Rohrs, A. Chattopadhyay, and R. Drechsler, Look-ahead schemes for nearest neighbor optimization of 1d and 2d quantum circuits, in *2016 21st Asia and South Pacific Design Automation Conference (ASP-DAC)* (2016) pp. 292–297.

[65] G. Li, Y. Ding, and Y. Xie, Tackling the Qubit Mapping Problem for NISQ-Era Quantum Devices, arXiv e-prints , arXiv:1809.02573 (2018), arXiv:1809.02573 [cs.ET].